

Rotational Friction Damper's Performance for Controlling Seismic Response of High Speed Railway Bridge-Track System

Wei Guo^{1,2}, Chen Zeng^{1,2}, Hongye Gou^{3,*}, Yao Hu^{1,2}, Hengchao Xu⁴
and Longlong Guo^{1,2}

Abstract: CRTS-II slab ballastless track on bridge is a unique system in China high speed railway. The application of longitudinal continuous track system has obviously changed dynamic characteristics of bridge structure. The bridge system and CRTS-II track system form a complex nonlinear system. To investigate the seismic response of high speed railway (HSR) simply supported bridge-track system, nonlinear models of three-span simply supported bridge with piers of different height and CRTS-II slab ballastless track system are established. By seismic analysis, it is found that shear alveolar in CRTS-II track system is more prone to be damaged than bridge components, such as piers, girders and bearings. The result shows that the inconsistent displacement of bridge girders is the main cause of the CRTS-II track system's damage. Then the rotational friction damper (RFD) is adopted, which utilizes the device's rotation and friction to dissipate seismic energy. The hysteretic behavior of RFD is studied by numerical and experimental methods. Results prove that RFD can provide good hysteretic energy dissipation ability with stable performance. Furthermore, the analysis of RFD's influence on seismic response of HSR bridge-track system shows that RFD with larger sliding force is more effective in controlling excessive inconsistent displacement where RFD is installed, though response of other bridge spans could slightly deteriorated.

Keywords: Rotational friction damper, high speed railway, simply supported bridge-track system, piers of different height, CRTS-II track system, seismic response control.

1 Introduction

Simply supported bridge with 32 m span prestressed concrete girder is generally taken as the standard construction bridge type and has been adopted as the main structure of China's high speed railway (HSR) bridges. Because of the longitudinal continuous CRTS-II slab ballastless track system, the dynamic characteristic of HSR bridge-track system has significantly changed [Cui, Guo, Su et al. (2019)]. In the study of train's moving safety and

¹ School of Civil Engineering, Central South University, Changsha, 410075, China.

² National Engineering Laboratory for High Speed Railway Construction, Changsha, 410075, China.

³ School of Civil Engineering, Southwest Jiaotong University, Chengdu, 610031, China.

⁴ Department of Civil Engineering, the University of British Columbia, Vancouver V6T 1Z4, Canada.

* Corresponding Author: Hongye Gou. Email: gouhongye@swjtu.edu.cn.

passenger's riding comfort, the train-track-bridge model [Gu, Liu, Guo et al. (2019); Hou, Li, Guo et al. (2018); Zhu, Gong, Wang et al. (2018); Liu, Yu and Guo (2019); Zhu, Gong, Wang et al. (2019)] is usually adopted and the interaction is analyzed by considering the track system as the elastic Bernoulli-Euler beam [Zeng, He, Zhao et al. (2015)]. However, by numerical analysis of HSR multi-span simply supported bridges, it has been concluded that piers and track system are easily damaged under seismic excitation [Yan, Liu, Pu et al. (2017); Guo, Zhai, Wang et al. (2019)]. Model test and in-situ test have been considered as the effective approach to systematically investigate the mechanical performance of HSR bridge structures [Gou, Yang, Leng et al. (2018); Gou, Yang, Mo et al. (2019)]. Shaking table test is a useful method to investigate seismic performance of structure system [Guo, Zhai, Wang et al. (2019)] and a shaking table test of 1/12 scaled HSR bridge specimen was performed, and it showed that the damage generally happened at the piers, bearings and track system [Kang, Jiang, Bai et al. (2017)]. There also exists collision between abutment and base plate in the simply supported bridges in different geography cases because of the non-uniform seismic excitation [Yan, Huang, Liu et al. (2018)]. The bearing is the key component in the bridge-track system, which is prone to be damaged [Dicleli and Bruneau (1995)] and can also adjust the force distribution of system [Kim, Mha and Lee (2006)]. Moreover, the track system is actually secondary system if the bridge system is considered as primary system, whose response characteristic is like that of pipeline [Li, Guo, Wang et al. (2019); Guo, Zhai, Wang et al. (2019)] attached to civil engineering structures. Together, these studies indicate that CRTS-II track system has obviously changed dynamic characteristics of HSR bridge system and is prone to damage, so the influence of CRTS-II track system must be considered when analyzing HSR bridge system. The damper is usually installed in buildings and bridges to control the seismic response and induce pounding, and here for HSR bridge the damper can be set in parallel with the movable bearing.

In order to mitigate the dynamic response of bridge, different devices have been investigated [Shrestha, Hao and Bi (2017)]. Tuned mass damper is designed to control vibration of high-pier bridges in Sichuan-Tibet railway induced by earthquake and running train [Chen, Han, Zhai et al. (2019)]. Passive supplemental damping devices including metallic damper, fluid viscous damper and friction pendulum bearing are considered to improve the longitudinal seismic performance of a steel cable-stayed bridge [Martínez-Rodrigo and Filiatrault (2015)]. A secondary linear oscillator is added along with underground rail tracks to suppress the low-frequency vibrations [Zhu, Yang, Yan et al. (2015)]. The railway bridge vertical vibration is controlled through magnetorheological damper by using fuzzy logic control algorithms, in this study, the railway bridge is modeled as Euler-Bernoulli beam and the damper is modeled as Bouc-Wen model [Mertin, Ulu, Paksoy et al. (2017)]. And, fluid viscous damper is found that it can give substantial reductions of the vertical acceleration of high-speed railway's deck [Rådeström, Ülker-Kaustell, Andersson et al. (2017)]. Also, a structure with three different dampers, viscoelastic damper, viscous damper and buckling-restrained brace is analyzed and result shows that seismic performance of different damper may be obviously different from each other [Guo, Wu, Hu et al. (2019)]. Overall, energy dissipating devices are effective to improve seismic response of bridge and building and to avoid pounding of adjacent structure [Liu, Yu and Guo (2019)]. However, it is noted that these studies did not consider longitudinal consistent slab track system that could influence the bridge response, the

response of bridge-track system is not well studied yet.

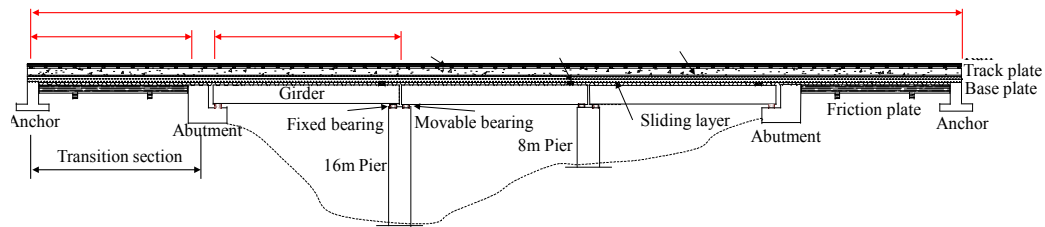
The development of friction dampers began in the late 1970s, and researchers have proposed a variety of energy absorption devices. Grigorian et al. [Grigorian, Yang and Popov (1993)] proposed a slotted-bolted connection energy dissipator designed to dissipate energy through friction. Pall et al. [Pall and Marsh (1982)] put forward a friction device applied in the steel framed buildings, and the friction joint with slotted holes can slide in the tension and compression state. Mualla et al. [Mualla and Belev (2015)] designed a friction damper, which is composed of three steel plates and two friction plates, and a bolt is used to connect three steel plates to each other and provide a normal force on the friction plates. Bi et al. [Bi, Hao and Chen (2018)] proposed a rotational friction hinge damper with spring to absorb the energy induced by the external vibration sources and to restore the original locations of pipe system. Kim et al. [Kim and Shin (2017)] developed a hybrid damper, which is made of a steel slit damper and rotational friction dampers and it is observed that the damper shows stable hysteretic behavior. An experiment of rotational friction damper has been conducted and results show that rotational friction damper has a suitable performance in moment resisting frames and damper with multi units should be employed to meet higher rotational strength demand with increasing building height [Mirzabagheri, Sanati, Aghakouchak et al. (2015)]. Also, rotational friction damper has been installed along with base isolation system for buildings, the results show that it can significantly reduce building displacement and base shear force [Barmo, Mualla and Hasan (2014)]. Rotational friction damper (RFD) [Mualla and Belev (2002)] has advantages of large hysteretic energy dissipation capacity, reasonable manufacturing and maintenance cost, which has been applied to control seismic response of the highway simply supported bridge [Shrestha, Hao, Ibrahim et al. (2016)] and buildings [Monir and Zeynali (2013)]. Overall, all of the studies reviewed here support that RFD has a high energy dissipation potential and easy installation and maintenance in structure. However, previous studies of rotational friction damper have not dealt with its effect in controlling seismic response of high-speed railway bridge-track system. This study focuses on evaluating the effectiveness of the RFD on mitigating the seismic response of high-speed railway bridge-track system. In this paper, seismic response and damage of HSR simply supported bridge-track system is studied firstly, and then the rotational friction damper (RFD) is introduced and studied by numerical and experimental work. By adopting RFD to control seismic response, parameter analysis is also carried out to figure out the influence of different sliding force. Finally, a numerical case study is given to study the performance of RFD to reduce the seismic response of HSR bridge-track system. The results show that shear alveolar is the key component among the bridge-track system; once its failure occurs, there exists excessive inconsistent displacement between adjacent girders. RFD has a good energy dissipation capacity and generally RFD with a large sliding force could improve the seismic performance of HSR bridge-track system.

2 Seismic response of HSR bridge-track system

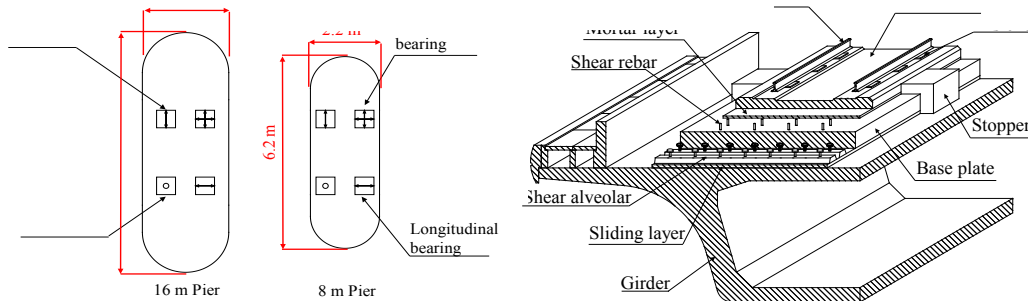
2.1 System description

Fig. 1(a) shows the longitudinal layout of HSR three span simply supported bridge-track system. It can be divided into two parts, the bridge system and CRTS-II track system. The

bridge system consists of piers, abutments, girders and bearings. The bridge is supported on two piers with different heights and two abutments. The round-shaped solid piers with large cross section are designed based on the stiffness to ensure the moving safety of train. The heights of two piers are 16 m and 8 m, respectively. The masses of piers are 879.5 tons and 251.2 tons, respectively. The girder with 32.6 m span and a 7.89 MN weight is simply supported by bearings including the longitudinal movable bearing, transverse movable bearing, bidirectional movable bearing and fixed bearing, as shown in Fig. 1(b). The bearing adopts the vertical design force of 5000 kN [Ministry of Railways (2004)]. The gap between adjacent bridge girders is 100 mm. The 50 m transition section between the subgrade and bridge system is set up to be the boundary condition. Transition section consists of friction plate, anchor and consistent base plate.



(a) The longitudinal diagram of bridge-track system



(b) Cross sections of 16 m pier and 8 m pier (c) The bridge girder and the track system

Figure 1: Detailed diagram of HSR bridge-track system

As shown in Fig. 1(c), the CRTS-II track system consists of sliding layer, base plate, mortar layer, track plate, fastener and rail, while it is connected to the simply supported girder by shear alveolar and sliding layer. The sliding layer which is located between the base plate and girder has a small friction coefficient and can reduce the restraint between track system and girder [Yan, Liu, Dai et al. (2016)]. Mortar layer is to support the track plate, adjust the height of the track slab and mitigate the dynamic responses under the train loading. Base plate, track plate and rail are continuous at the longitudinal direction of the HSR bridge. The shear alveolar, which locates near fixed bearings to connect base plate and girder, is mainly to transmit superstructure forces to girder. Shear rebar is located at ends of base plate to combine track plate and base plate.

2.2 Numerical model

To study the control performance of RFD in the seismic response of HSR three span simply supported bridge-track system, nonlinear numerical models are established by OpenSees. Girder, base plate, track plate and rail are modeled using elasticBeamColumn element and the detailed description of elasticBeamColumn element (EBC) is shown in Tab. 1 [Yan, Dai and Hu (2015)]. Bearing, sliding layer, mortar layer, fastener, shear alveolar and shear rebar are modeled using ZeroLength element, and force-displacement relationships of ZeroLength elements are given in Tab. 2. The rotation material of sliding layer, CA mortar layer, fastener is elastic, which has a large stiffness 1×10^{10} kN*mm/mm⁻¹. Movable bearing's rotation material is elastic with a small stiffness 1×10^{-10} kN*mm/mm⁻¹. And each pier is modeled using ZeroLength element and rigid beam with the relationship between moment and curvature at the pier bottom. The hysteretic model of piers is given by Pinching4 material by fitting the experimental data of pier's cyclic tests [Jiang, Shao, Jiang et al. (2013)]. The experiment data and hysteretic numerical models of 16 m and 8 m piers are shown in Fig. 2. The friction plate, as the bridge transition section, is embedded into the crushed rock embankment which is simulated by ZeroLength Element. The longitudinal stiffness of the crushed rock embankment is 150 kN/mm, and its vertical stiffness is 1×10^6 kN/mm [Zhu, Dai and Yan (2014)]. Piers are fully fixed on the foundation.

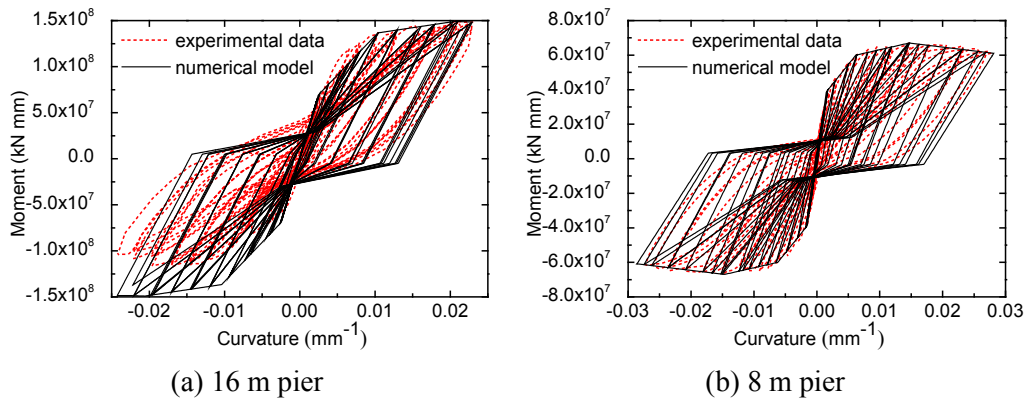
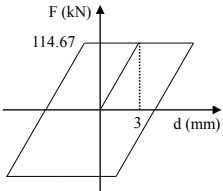
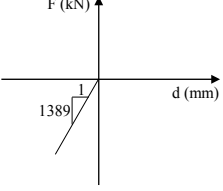
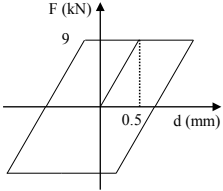
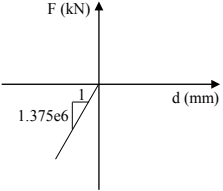
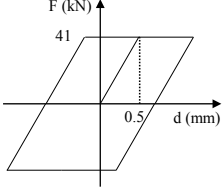
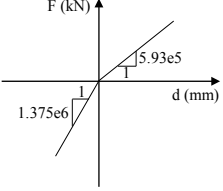
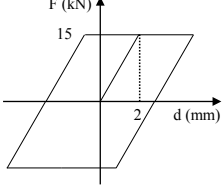
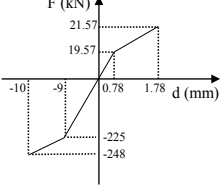
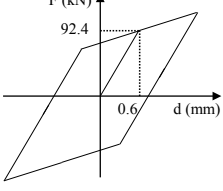
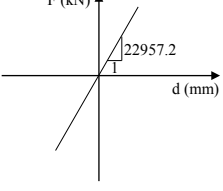
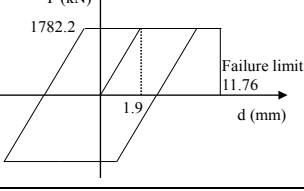
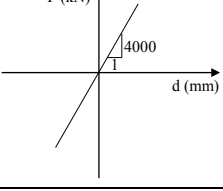


Figure 2: The hysteretic models of two piers

Table 1: Parameters of elasticBeamColumn elements

| Components | Section Area (mm ²) | Elastic Modulus (N/mm ²) | Moment of area (mm ⁴) | Density(kg/m) |
|----------------|---------------------------------|--------------------------------------|-----------------------------------|---------------|
| Girder | 8.343×10^6 | 4.4×10^4 | 9×10^{12} | 22691 |
| Base plate | 5.60×10^5 | 3.25×10^4 | 1.68×10^9 | 1496.85 |
| Track plate | 5.10×10^5 | 3.6×10^4 | 1.70×10^9 | 1370.6 |
| Rail | 7.75×10^3 | 2.1×10^5 | 3.2×10^7 | 60.64 |
| Friction plate | 3.60×10^6 | 3.0×10^4 | 4.8×10^{10} | 9360 |

Table 2: Force-displacement relationships of ZeroLength elements

| Components | Longitudinal direction | Vertical direction |
|-----------------|---|---|
| Movable bearing |  |  |
| Sliding layer |  |  |
| Mortar layer |  |  |
| Fastener |  |  |
| Shear rebar |  |  |
| Shear alveolar |  |  |

In Tab. 2, the longitudinal force-displacement relationship of the sliding layer is given by the elastic-plastic model. The friction coefficient is 0.3, the sliding displacement is 0.5 mm and the friction force is 9 kN [Ren, Li, Yang et al. (2016)]. The vertical stiffness is 1.376×10^5 kN/mm in compression and zero in tension, as sliding layer can only endure compression. The longitudinal force-displacement relationship of the mortar layer is similar to sliding layer. The vertical compressive and tensile stiffness are 2×10^6 kN/mm

and 5.93×10^5 kN/mm, respectively. The longitudinal stiffness of each fastener is 15 kN, and the elastoplastic critical displacement is 2 mm. Fastener's vertical stiffness depends on its working state and stiffness of elastic strip [Zhu, Dai and Yan (2014)].

The shear alveolar is modeled by the elastic-plastic model and the elastoplastic critical displacement is 1.9 mm. The MinMax material is adopted to simulate the failure when the maximum deformation exceeds 11.76 mm. The shear alveolar keeps elastic with stiffness equal to 22957.2 kN/mm in the vertical direction. The elastic-plastic model is also adopted to describe the force-displacement relationship of the shear rebar. The yield displacement is 0.6 mm. The shear rebar maintains elastic in the vertical direction, and the stiffness is 4000 kN/mm. The finite element model is shown in Fig. 3.

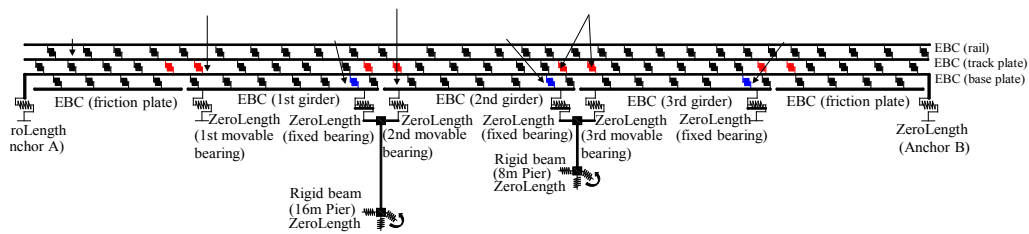


Figure 3: Finite element model for three-span simply supported HSR bridge-track system

2.3 Nonlinear time history analysis

The seismic fortification intensity is assumed to be 8 degree in China's code [Ministry of Construction (2006)] and corresponding seismic peak ground acceleration A_g is 0.3 g. The ground motion record is given and shown in Fig. 4 and Tab. 3. The peak acceleration corresponding to each seismic intensity is scaled to be 0.099 g for the frequent earthquake, 0.3 g for the design earthquake, 0.63 g for the rare earthquake [Ministry of Construction (2006)].

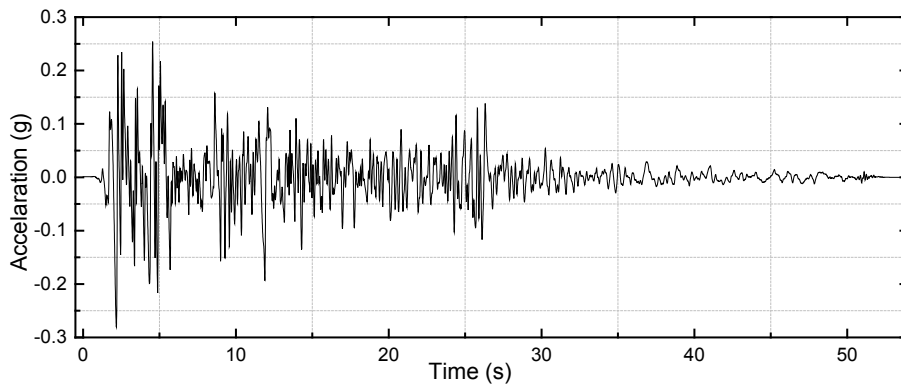


Figure 4: Selected ground motion record for time history analysis

Table 3: Ground motion record information

| Earthquake | Station information | Mechanism | Magnitude |
|--------------------------|--------------------------|-------------|-----------|
| Imperial Valley-02, 1940 | El Centro Array #9, 180° | Strike slip | 6.95 |

The seismic response of HSR three span simply supported bridge is discussed here. As it can be seen in Fig. 5(a), the 16 m pier’s deformation is more obvious than 8 m piers. The deformation difference between 16 m pier and 8 m pier significantly increases in the rare earthquake. The 16 m pier presents nonlinearity as shown in Fig. 5(b). Piers with different heights have different natural vibration characteristics and different seismic responses. Also, in the rare earthquake, the displacements of the 1st and 2nd movable bearings obviously increase and exceed the failure limit, which means the failure of movable bearings as shown in Fig. 5(c). Movable bearings can dissipate part of seismic energy, which is shown in Fig. 5(d).

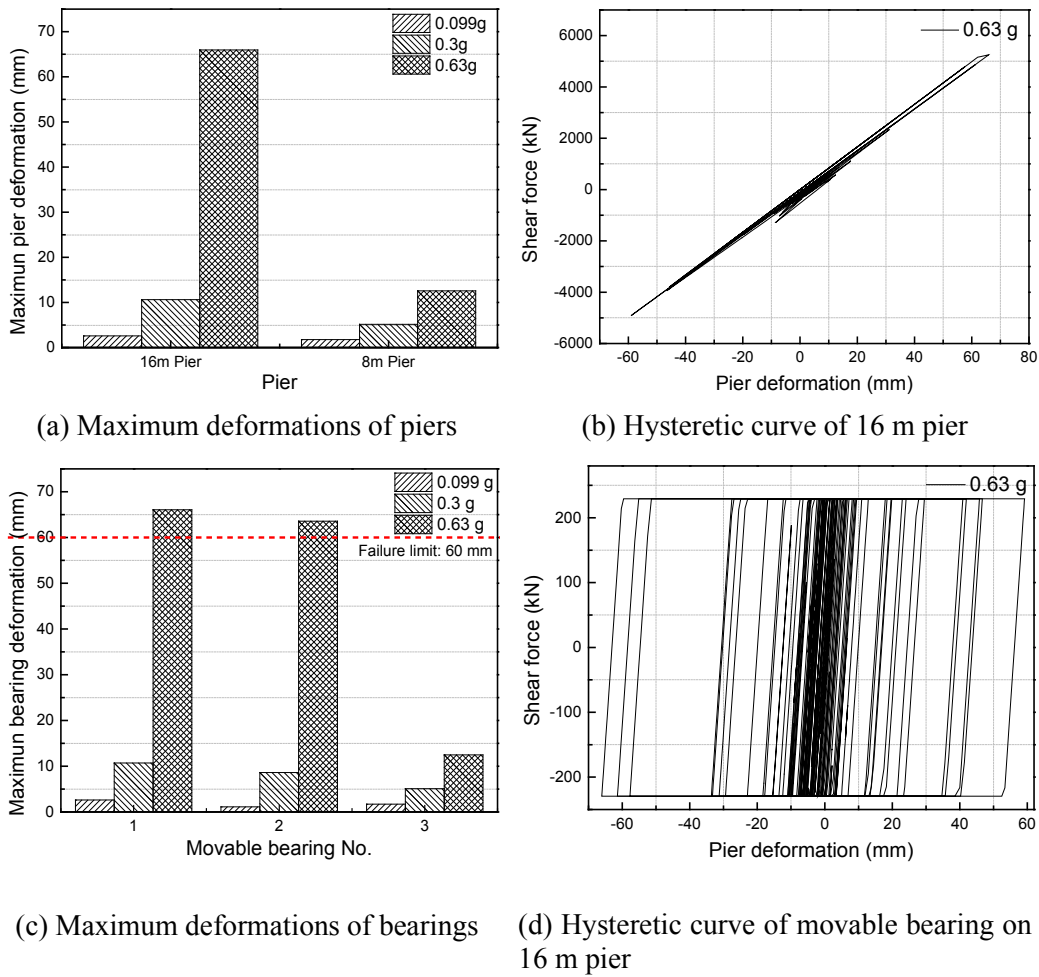


Figure 5: Seismic response of piers and movable bearings

As seen in Fig. 6(a), the longitudinal deformation of CRTS-II track system varies along the bridge span. The longitudinal displacement response of sliding layer is generally large compared to other components of the CRTS-II track system, and changes obviously near the movable bearings of each simply supported girder and the maximum value reaches to 66.65 mm in the 1st girder while the seismic intensity is 0.63 g. The shear alveolar is

damaged under 0.63 g seismic excitation as shown in Fig. 6(b). The deformations of mortar layer are within 0.5 mm limit at most positions, despite that position near each anchor, where the deformations of mortar layer are relatively large as shown in Figs. 6(c)-6(d). Shear rebars and fasteners remain elastic.

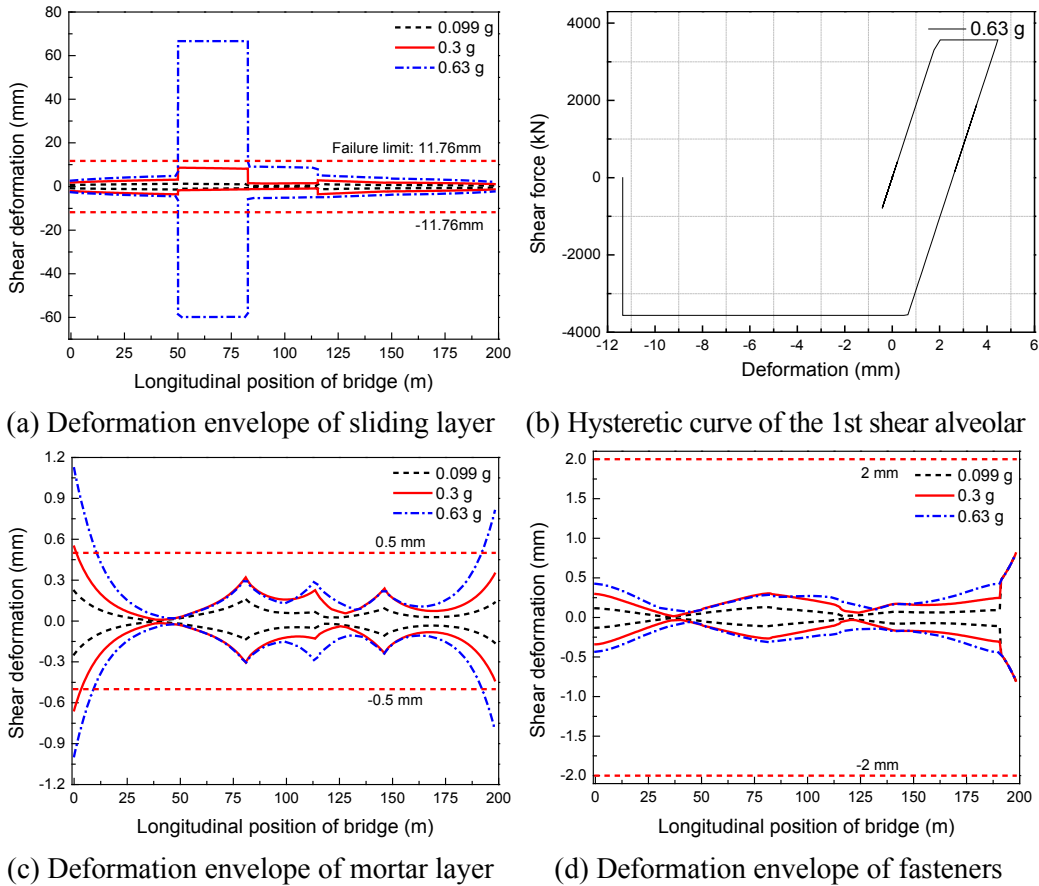


Figure 6: Longitudinal deformation response properties of CRTS-II track system

In addition, sliding layer is damaged even in the frequent earthquake of 0.099 g, and the deformation along the bridge exceeds 0.5 mm limit. Because of small friction coefficient of sliding layer, the sliding between base plate and girder is easy to happen. Shear alveolar is placed along with sliding layer, it has a limit deformation with the value of 11.76 mm. The shear alveolar usually remains elastic and has no damage in the frequent and design earthquake, and from Fig. 6(b), it reveals that in the rare earthquake, the shear alveolar at the 1st girder exceeds the limit value and its failure occurs.

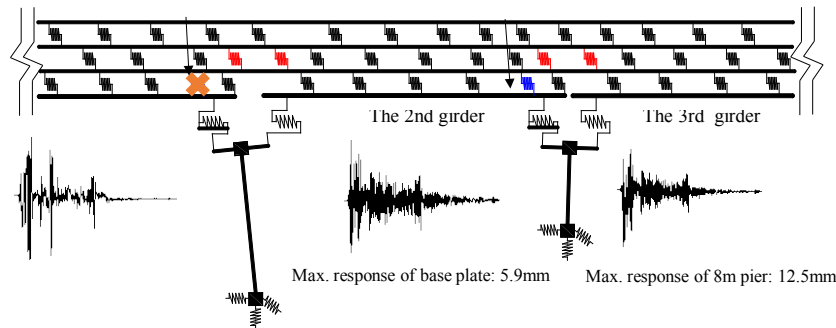


Figure 7: Damage mechanism diagram of bridge-track system

In the rare earthquake, the shear alveolar in the 1st girder is completely damaged, as shown in Fig. 7. The shear alveolar has the function of connecting base plate of CRTS-II track system and bridge girder with a large stiffness of 3561 kN/mm. The shear alveolar provides more resisting force, that is 3564 kN, than the total resisting force 1930 kN by sliding layer in one girder.

As shown in Fig. 7, base plate has the minimum deformation because of the longitudinal consistent distribution and anchor with large stiffness. Once shear alveolar fails, there's actually little connection between girder and base plate, and only the friction in sliding layer plays a role. Then the different vibration period of 8 m and 16 m pier produce an obvious inconsistent displacement of adjacent girders. In fact, CRTS-II track system is like a secondary system attached to the bridge system. Because of its longitudinal continuous feature, CRTS-II track system has a strong constraint effect on the simply supported bridge. Sliding layer and shear alveolar are the only components between bridge girder and CRTS-II track system, so they are key components in bridge-track interaction. Sliding layer is easy to slide because of its small friction coefficient. As shown in Fig. 8, both in frequent and design earthquake, the 1st shear alveolar has no damage. Also, the 1st shear alveolar and movable bearings have a similar displacement time history because shear alveolar connect CRTS-II track system and bridge girder, bridge vibrates with CRTS-II track system's restriction. However, in rare earthquake, displacement of shear alveolar exceeds the failure limit. Without the strong restriction of the 1st shear alveolar, the 1st girder starts to vibrate with 16 m pier, which results in inconsistent displacement of bridge girders. The 1st shear alveolar fails at 2.215 s and without shear alveolar restriction, the 1st and 2nd movable bearings exceed the limit displacement at 5.29 s and 5.35 s, respectively. As a result, shear alveolar plays an important role in HSR bridge-track system. Also, shear alveolar has a small failure limit and it first breaks down in the entire bridge-track system. Once shear alveolar is damaged, it is difficult to be replaced and repaired. In this paper, the rotational friction damper (RFD) is adopted to improve the seismic performance of HSR three span simply supported bridge.

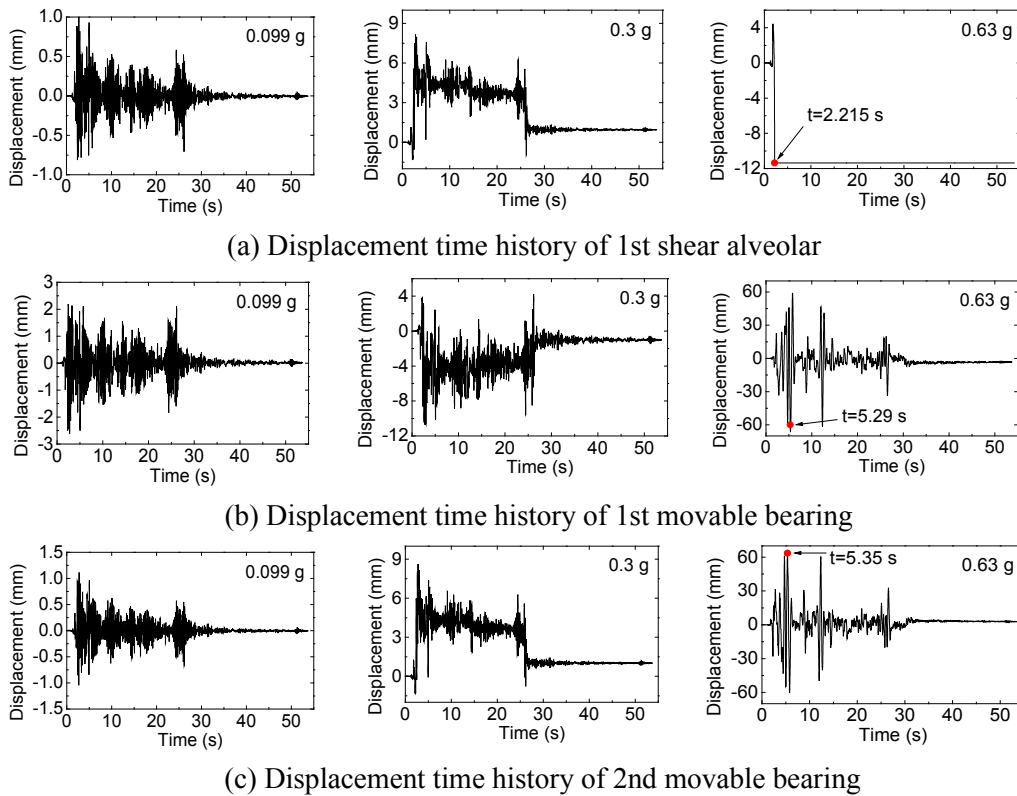


Figure 8: Displacement time history of shear alveolar and movable bearing

3 Rotational friction damper

3.1 Mechanism of RFD

Many types of friction dampers have been applied in the steel and concrete building structure to control the seismic response. Here, rotational friction damper (RFD) [Shrestha, Hao, Ibrahim et al. (2016)] is introduced to mitigate the seismic damage of HSR simply supported bridge and the longitudinally continuous track-slab system. One unit of RFD consists of three steel plates rotating against each other and between every two steel plates, there is a friction plate made of friction materials in order to provide stable dry friction force as seen in Fig. 9(a). The bolt connects steel plates and friction plates as a rotational unit and the normal force applied on the friction plate can be controlled by adjusting the bolt's clamping force. The relative motion of two hinges generates friction force in the friction surfaces between steel plates and friction plates. RFD stays in stuck until the force F transferred to the damper is larger than the friction force, and then steel plates begin rotating relatively to the friction plate around the bolt. RFD dissipates external energy in form of friction. According to the requirement of seismic response control, RFD can be combined to have multiple friction surfaces, that is shown in Fig. 9(b).

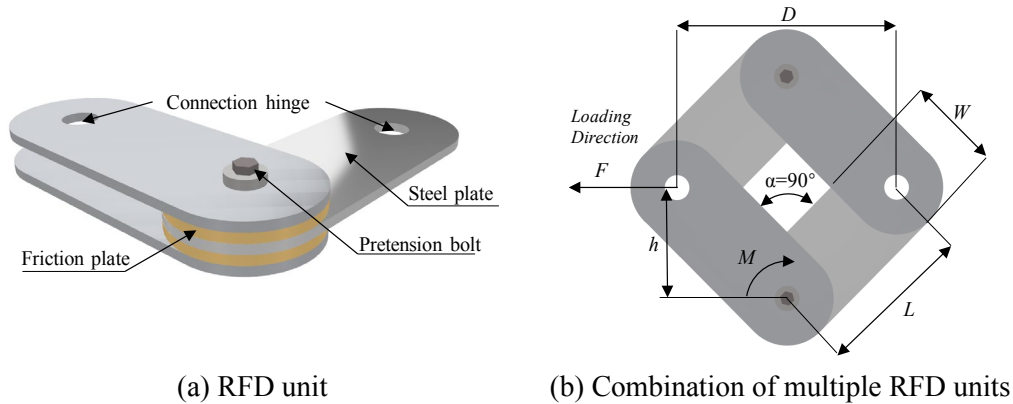


Figure 9: Scheme of rotational friction damper

To investigate the mechanism of RFD, the sliding friction force of RFD is explained firstly. The main physical parameters of RFD include length L , width W and thickness t , the angle between adjacent steel plates is α . The sliding friction force F can be calculated by structural force analysis as follows:

$$n \cdot M = F \cdot h \tag{1}$$

Based on the geometry of the damper as seen in Fig. 1(b), Eq. (1) can be rewritten as:

$$F = \frac{n \cdot M}{\sqrt{L^2 - (D/2)^2}} \tag{2}$$

The number of the friction surface in RFD is assumed to be n . M is the friction moment of one friction surface after applying pretension force. h is the arm of force between sliding friction force F and pretension bolt axis. D is the distance between two connection hinges. In the sliding phase, since friction force is produced by the relative rotation of the friction surface, the relationship between friction force and rotation needs to be established. While the angle of the rotation is related to horizontal displacement of two connection hinge, the sliding force F can be calculated based on the relations given by Shrestha et al. [Shrestha, Hao and Ibrahim (2016)] and Monir et al. [Monir and Zeynali (2013)].

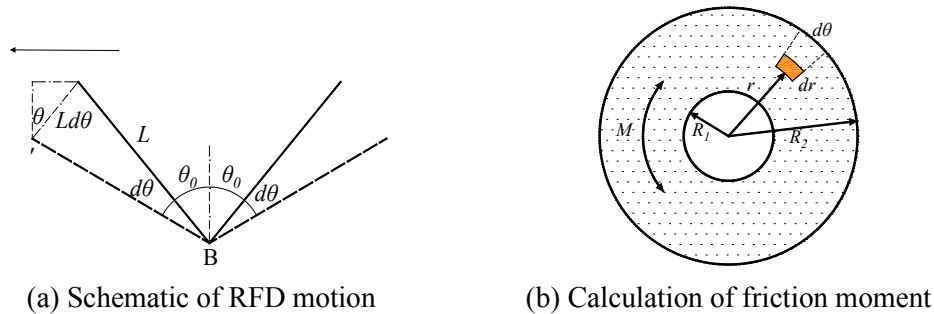


Figure 10: Scheme of RFD's mechanism

In Fig. 10, point B represents the position of the rotation axis, and point A is the loading position of horizontal external force. Suppose that the damper has a $2d\theta_0$ initial rotation angle which is equal to α . Under the external force, each steel plate has $d\theta$ rotation angle relative to the original position. Thus, connection hinge A produces a horizontal displacement Δx ($\Delta x=Ld\theta\cos\theta$) due to the rotation at point B, so the total horizontal displacement of the damper is $2Ld\theta\cos\theta$. Using energy conservation method, the work done by the horizontal force is equal to the work done by the frictional bending moment of the friction damper as shown in Eq. (3).

$$F \cdot 2Ld\theta \cdot \cos\theta = n \cdot M \cdot 2d\theta \tag{3}$$

According to the geometry of the damper as shown in Fig. 10(a), the relationship between the rotation angle and horizontal displacement can be built in Eq. (4).

$$\sin\theta = \frac{\Delta x / 2 + L \cdot \sin\theta_0}{L} \tag{4}$$

The friction moment in the friction damper can be integrated by the area of the friction surface as shown in Fig. 10(b).

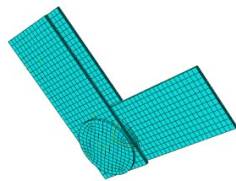
$$M = \mu \cdot \sigma_0 \cdot \int_0^{2\pi} \int_{R_1}^{R_2} r^2 dr d\theta \tag{5}$$

where, σ_0 represents the pressure distributed on the friction surface, and R_1 represents the inner diameter of the friction surface, and R_2 represents the outer diameter of the friction surface, and the sliding friction force F can be given by:

$$F = \frac{n \times \mu \times \sigma_0 \times \int_0^{2\pi} \int_{R_1}^{R_2} r^2 dr d\theta}{L \times \sqrt{1 - \left(\frac{\Delta x}{2L} + \sin\theta_0\right)^2}} \tag{6}$$

3.2 Numerical simulation and experiment

In order to figure out the actual performance of RFD, the numerical simulation and experiment are both carried out. A numerical model is developed using the commercial finite element software package ABAQUS. Considering the geometric symmetry, the RFD unit is adopted. By simplifying the bolt into a rotation axis, the pretightening force is simulated using a uniform pressure applied to the circular gasket. Surface to surface contact is adopted to simulate the friction moment. The finite element model of RFD is shown in Fig. 11(a).



(a) Finite element model of RFD unit

(b) RFD specimen

Figure 11: Numerical model and experimental specimen of RFD

The RFD specimen is shown in Fig. 11(b). The type of steel is Q345 and the steel plates are machined to exact dimensions as shown in Tab. 4. The friction plate is made up of copper. Then steel plates and friction plates are assembled into RFD using two high-strength bolts. The coefficient of metal friction between steel and copper is 0.35. According to the relationship between bolt moment and bolt axial force as shown in Eq. (7), the bolt tightening torque in RFD specimen and the uniform pressure in RFD numerical model can be adjusted.

Table 4: Specifications of RFD specimen

| D (mm) | W (mm) | L (mm) | t (mm) | α (°) |
|--------|--------|--------|--------|--------------|
| 353.5 | 150 | 250 | 12 | 90 |

$$T = 1.25 f P_0 d \quad (7)$$

where, T is the bolt tightening torque; f is the friction coefficient of bolt nut and the plate; P_0 is the preloading axial force and d is the bolt nominal diameter [Ruan (1985); Dong (2017)].

The axial hysteretic curve of RFD can be tested by loading of a hydraulic actuator. One side of RFD is attached to the reaction wall and the other side is connected to actuator, which is shown in Fig. 12. A linear variable differential transformer (LVDT) is installed between the actuator and the specimen to measure the actual deformation of RFD specimen. Also, a force transducer is installed in the actuator to obtain the resisting force of RFD specimen.



Figure 12: Experimental setup of RFD specimen

3.3 Test results

The behavior of RFD can be divided into two stages: the stuck stage and sliding stage. In the stuck stage, the force transferred to RFD is smaller than the friction force produced by the friction surface between steel plates and friction plates and RFD behaves elastic with stiffness of 10 kN/mm. In the sliding stage, the force transferred to RFD overcomes the design sliding force and friction plates move relatively against steel plates. The resisting force of RFD changes with the displacement. Corresponding to Eq. (1), the frictional moment of RFD is determined by the friction coefficient and the dimension of friction plate, and h is related to the RFD deformation, so the force F changes with the displacement between two connection hinges.

Hysteretic curves of RFD are shown in Fig. 13. RFD presents asymmetric hysteretic loops and exhibits different response characteristics in tension and compression. While loading

in the reverse direction, there exists displacement drift due to gap of RFD specimen installation. The sliding force of each cycle does not change much.

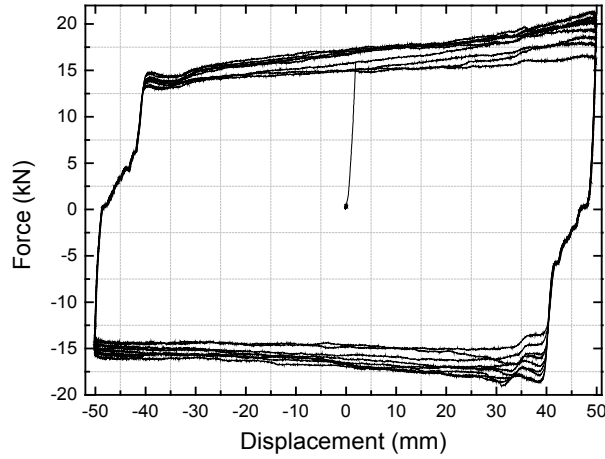


Figure 13: Force-displacement curve of RFD's experiment

Dissipated energy of RFD over a loading cycle can be expressed by:

$$E_i = \int F_i |\Delta| dt \tag{8}$$

where, E_i is the dissipated energy in the i th loading cycle, and F is the resisting force of RFD during the i th loading cycle and Δ is the deformation of RFD. Tab. 5 shows the dissipated energy of each cycle, and the maximum deviation from average is 8.21% in the 2nd loading cycle. It indicates that RFD has a stable energy dissipation capacity.

Table 5: Dissipated energy for each cycle of loading

| Cycle No. | Dissipated energy (J) | Deviation from average (%) |
|-----------|-----------------------|----------------------------|
| 1 | 2777 | 6.25 |
| 2 | 2719 | 8.21 |
| 3 | 2859 | 3.48 |
| 4 | 2978 | 0.54 |
| 5 | 3057 | 3.20 |
| 6 | 3060 | 3.30 |
| 7 | 3078 | 3.91 |
| 8 | 3138 | 5.94 |
| 9 | 2993 | 1.04 |
| Average | 2962 | |

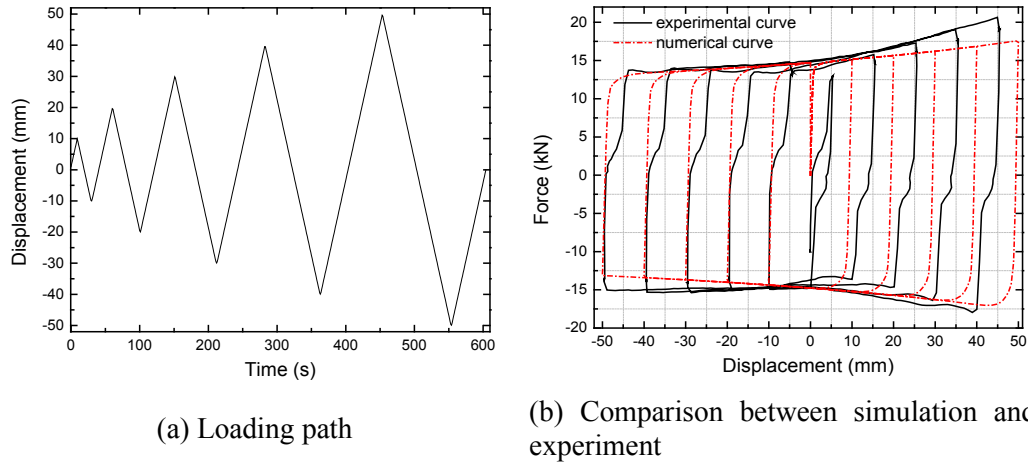


Figure 14: Hysteretic curve of RFD under cyclic loading

Previous research indicated that friction damper has the bilinear behavior [Mualla and Belev (2002)]. It is very common to describe the friction damper using rigid plastic or elastic perfectly-plastic material in numerical simulation [Bhaskararao and Jangid (2006)]. According to experimental result, the numerical model of RFD specimen can be generalized, the initial stiffness of RFD is 10 kN/mm with 1.5 mm elastic displacement. The starting sliding force is 15 kN and post-yield stiffness of zero is adopted.

4 Performance of RFD applied in HSR Bridge-track system

Test result shows that the performance of RFD is stable and RFD provides a good energy dissipation capacity with a long stroke. These characteristics of RFD make it helpful to improve seismic performance of HSR three-span simply supported bridge as discussed before. Results of analysis of high-speed railway bridge shows that once the 1st shear alveolar fails, 16 m pier could produce a large displacement response, which results in large deformation in movable bearing and inconsistent displacement between adjacent girders. Considering RFD has a simple mechanism, it can be easily assembled to meet different seismic demands. RFD is installed in the longitudinal direction to reduce longitudinal relative displacement of bridge structures.

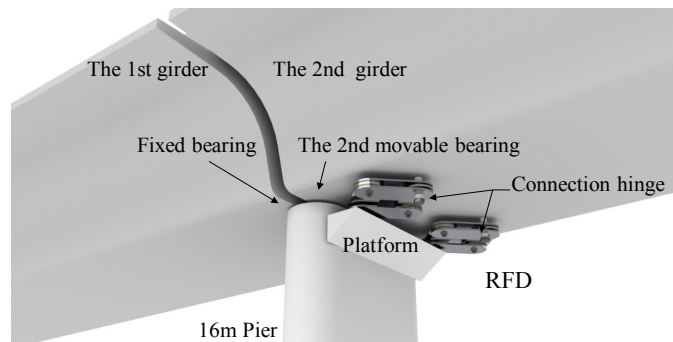


Figure 15: Connection scheme for RFD

As shown in Fig. 15, two ends of RFD are connected to pier and girder of the bridge along with the movable bearing to mitigate inconsistent displacement between the 1st and 2nd girders. Moreover, a lock-up viscous device could be installed with the RFD so that bridge allows slow displacements, like temperature expansion, concrete shrinkage and creep and transfer the shocks to RFD under high frequency movements when bridge is subjected to earthquake. Bilinear model is utilized to describe the RFD with a high initial stiffness in stuck stage and begins sliding when the force in RFD exceeds sliding friction force with zero stiffness. The response of three span simply supported bridge equipped with RFD under rare earthquake of 0.63 g is discussed as follows.

4.1 RFD's influence on seismic response

In order to figure out the influence of RFD's sliding force on seismic response of three span simply supported bridge-track system, analysis is carried out considering different sliding forces. According to the mechanism of RFD, the sliding force could be controlled by changing bolt pretension torque or adjusting the number of friction plates, so several RFDs could be installed in parallel to provide large force and energy consumption capacity. In this section, the total force of the damper with several RFD units can be regarded as F_T and can be calculated in Eq. (9), and m is the number of RFD.

$$F_T = n \cdot 15kN, k_T = n \cdot 15kN / 1.5mm \tag{9}$$

In this section, six dampers' force F_T , i.e., 450, 900, 1350, 1800, 2250 and 2700 kN are taken into consideration to analyze the influence of different sliding force. These are defined as the damper force F_T over weight of simply supported girder of 10%, 20%, 30%, 40%, 50% and 60%, respectively.

As shown in Fig. 16(a), with the force increasing, 16 m pier's deformation is decreasing, while 8 m pier's deformation slowly increase. The increase of RFD's force changes from 2250 kN to 2700 kN, and has insignificant effect on reducing 16 m pier's deformation. As shown in Fig. 16(b), the deformation of the 1st and 2nd movable bearings decrease with the increasing of RFD's force and both are within the failure limit with 60 mm. Also, the 3rd movable bearing's deformation increase because 8 m pier's deformation increase.

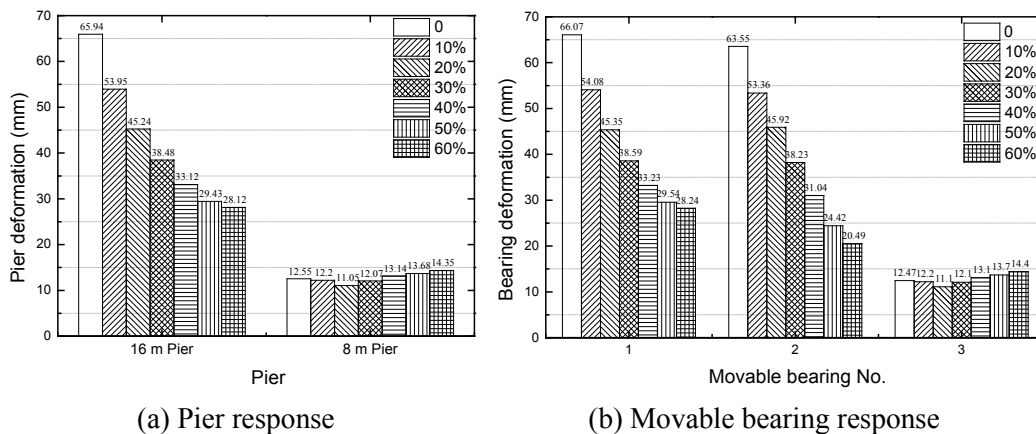


Figure 16: Pier and Movable bearing deformation

The energy dissipated by RFD is influenced by the damper's sliding force. Fig. 17 shows the hysteretic curve of RFD with sliding force 10% and 60%. It is obvious that RFD quickly began working in earthquake due to its small elastic displacement (1.5 mm). It is also observed that the increasing sliding force can control RFD's deformation, then the deformation of movable and the bridge girder can be controlled. In this study, RFD is installed on 16 m pier, the response of 16 m pier can be directly decreased, as a result, the displacement of the 1st girder connected with 16 m by fixed bearing and the 2nd movable bearing can be controlled; however, increase in sliding force could result in increase in other parts of the bridge, the 8 m pier and the 3rd movable bearing, this is because RFD not only plays a role in energy dissipation, but also can adjust the internal force distribution in the structure; unlike movable bearing's isolation effect, RFD transfer more seismic force from 16 m pier to 8 m pier, which makes 8 m pier's deformation increasing. Therefore, sliding force of RFD applied in HSR bridge should be carefully considered for better performance of the whole bridge-track system.

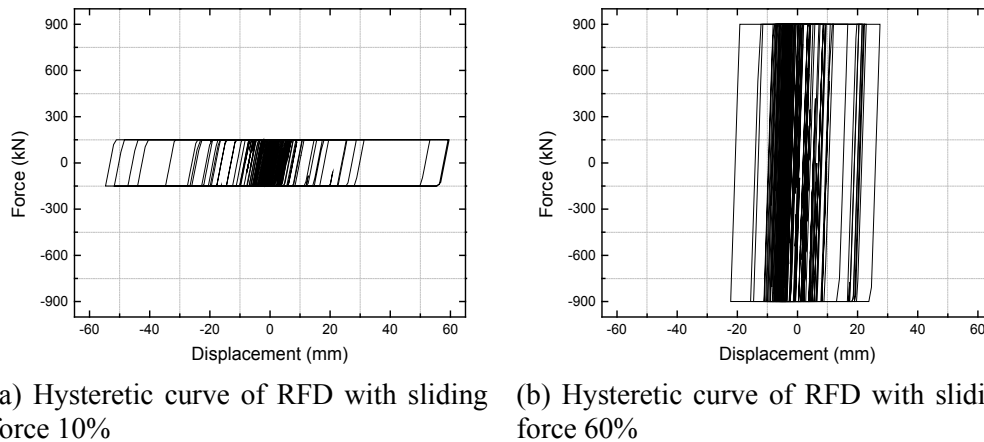


Figure 17: Comparison of hysteretic curve of RFD with different sliding force

As shown in Fig. 18(a), the maximum deformation of sliding layer in the 1st girder decreases obviously, but it also shows that there is not much difference in RFD's force with 50% and 60%. Although the maximum deformation of sliding layer is decreasing, the 1st shear alveolar still fails under the large deformation against the failure limit. As shown in Fig. 18(b), the maximum deformation of sliding layer in the 2nd girder increases slightly. Before the 1st shear alveolar fails, RFD starts working to dissipate seismic energy; once the 1st shear alveolar fails, RFD continues to work. By taking the place of shear alveolar after its failure. RFD not only dissipate seismic energy, but also connects the 1st and 2nd simply supported girders.

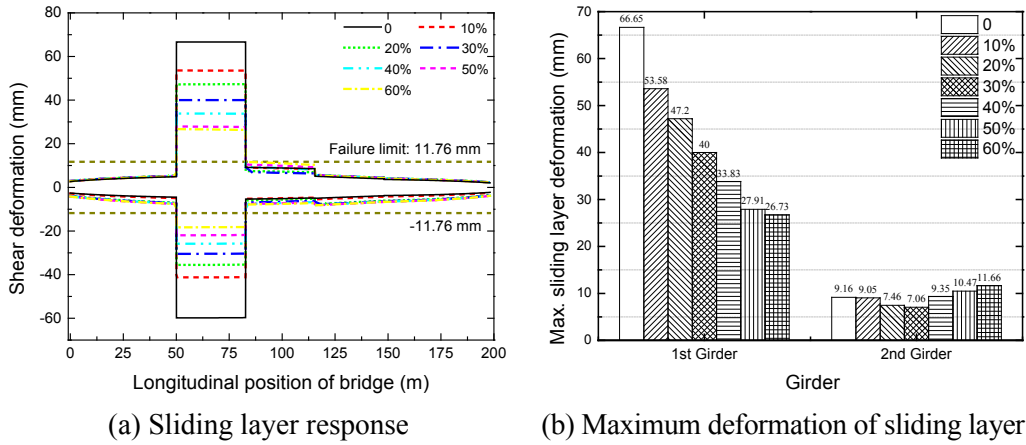


Figure 18: Response of sliding layer of track system

4.2 Performance of RFDs

The performance of HSR three span simply supported bridge is compared in terms of pier deformation, movable bearing deformation and residual displacement and response of shear alveolar. The situation of RFD's force with 900 kN is discussed here.

With the application of RFD on HSR bridge-track system, the response of the 1st shear alveolar is shown in Fig. 19. Compared with bridge without RFD, the response of the 1st shear alveolar has a larger hysteretic loop, which means the 1st shear alveolar has a longer operating time. RFD are installed along with the 2nd movable bearing, so they have same shear deformation.

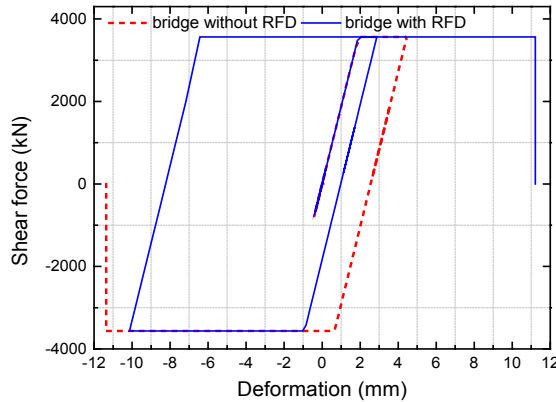
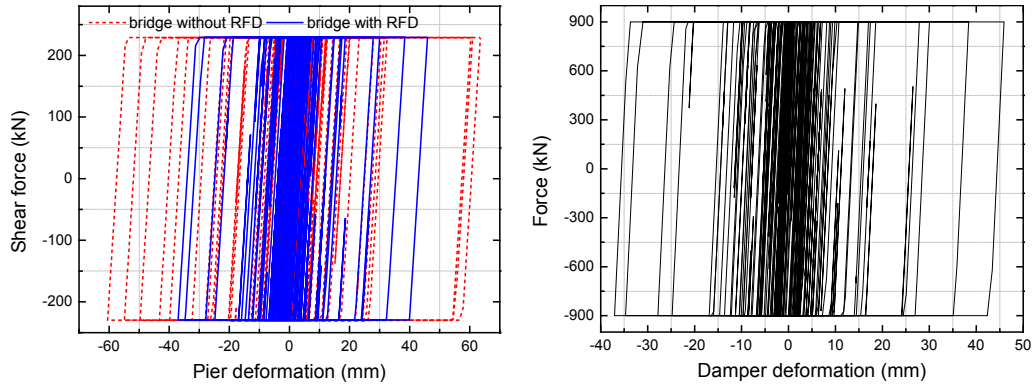


Figure 19: The 1st shear alveolar hysteretic curve

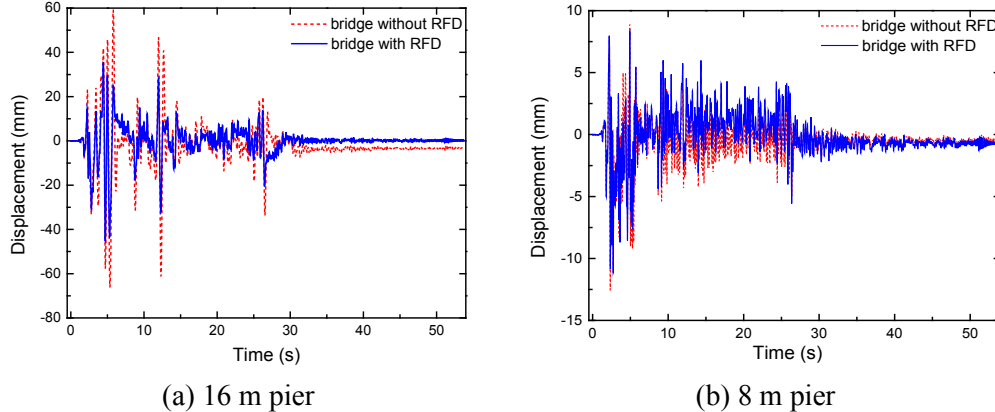


(a) The 2nd movable bearing hysteretic curve

(b) Hysteretic curve of damper

Figure 20: Response of bearing and RFD

As shown in Fig. 21, the advantages of using RFD to control inconsistent displacement response are obvious. The 16 m pier deformation has been decreased from 65.94 mm to 47.20 mm. Also, the residual deformation of 16 m pier is reduced by RFDs. Application of RFD in the HSR simply supported bridge can decrease the inconsistent displacement of adjacent girders, and it can control the deformation of 16 m pier and dissipate energy, while it only leads to slight decrease of response of 8 m pier.



(a) 16 m pier

(b) 8 m pier

Figure 21: Response of piers of HSR simply supported bridge

5 Conclusions

This paper focuses on the RFD to improve seismic response of HSR three span simply supported bridge. The bridge model is based on the real HSR lines and the bridge-track system is established with continuous CRTS-II track system. It found that shear alveolar with large deformation is more likely to fail in rare earthquake compared with other components in CRTS-II track system and bridge structures. It shows that CRTS-II track system has a great constraint effect on simply supported bridge girders, but the connection

between CRTS-II track system and bridge system is seismic vulnerable because of large inconsistent displacement of adjacent girders in rare earthquake. Numerical and experimental tests of RFD show that RFD has a good energy dissipation capacity and its performance is stable. According to results in this paper, RFD is adopted to improve the seismic response of HSR bridge. Sliding force of RFD is a key parameter for better control seismic performance of bridge-track system. RFD can effectively mitigate seismic response where it is installed. However, increasing sliding force of RFD could slightly increase response of other pier in bridge because more seismic force is transferred to pier. The result shows that RFD is effective in mitigating inconsistent displacement between adjacent girders. Although shear alveolar could fail when RFD is applied, RFD can not only dissipate seismic energy, but also connects simply supported girders by adjust the internal force among them. In a case study, the sliding force is initially determined, the result shows that the maximum deformation of 16 m pier is reduce to 45.24 mm from 65.94 mm while the response of 8 m pier is only decreased from 12.55 mm to 11.05 mm; the movable bearings' response is controlled within failure limit. The results of this study indicate that RFD is generally effective to improve seismic performance of HSR simply supported bridge-track system.

Acknowledgement: The authors are grateful for the financial support from the Fundamental Research Funds for the Central Universities of Central South University (Project No. 502221804), the National Natural Science Foundation of China (Project Nos. 51878674, 51878563), the Foundation for Key Youth Scholars in Hunan Province (Project No. 150220077) and the Project of Yuying Plan in Central South University (Project No. 502034002). Any opinions, findings, and conclusions or recommendations expressed in this paper are those of the authors.

References

- Barmo, A.; Mualla, I. H.; Hasan, H. T.** (2014): The behavior of multi-story buildings seismically isolated system hybrid isolation (friction, rubber and with the addition of rotational friction dampers). *Open Journal of Earthquake Research*, vol. 4, no. 1, pp. 1.
- Bhaskararao, A. V.; Jangid, R. S.** (2006): Seismic response of adjacent buildings connected with friction dampers. *Bulletin of Earthquake Engineering*, vol. 4, no. 1, pp. 43-64.
- Bi, K.; Hao, H.; Chen, W.** (2018): Effectiveness of using RFHDS connected PIP system for subsea pipeline vibration control. *International Journal of Structural Stability and Dynamics*, vol. 18, no. 8, 1840005.
- Chen, Z.; Han, Z.; Zhai, W.; Yang, J.** (2019): TMD design for seismic vibration control of high-pier bridges in Sichuan-Tibet railway and its influence on running trains. *Vehicle System Dynamics*, vol. 57, no. 2, pp. 207-225.
- Cui, S.; Guo, C.; Su, J.; Cui, E.; Liu, P.** (2019): Seismic fragility and risk assessment of high-speed railway continuous-girder bridge under track constraint effect. *Bulletin of Earthquake Engineering*, vol. 17, no. 3, pp. 1639-1665.

- Dicleli, M.; Bruneau, M.** (1995): An energy approach to sliding of single-span simply supported slab-on-girder steel highway bridges with damaged bearings. *Earthquake Engineering & Structural Dynamics*, vol. 24, no. 3, pp. 395-409.
- Dong, D.; Chen, J.; Liu, H.; Mei, X.** (2017): Research on torque coefficient of high-strength bolt. *Science Technology and Engineering*, vol. 17, no. 16, pp. 182-186.
- Gou, H. Y.; Wang, W.; Shi, X. Y.; Pu, Q. H.; Kang, R.** (2018): Behavior of steel-concrete composite cable anchorage system. *Steel and Composite Structures*, vol. 26, no. 1, pp. 115-123.
- Gou, H. Y.; Yang, L. C.; Leng, D.; Bao, Y.; Pu, Q. H.** (2018): Effect of bridge lateral deformation on track geometry of high-speed railway. *Steel and Composite Structures*, vol. 29, no. 2, pp. 219-229.
- Gou, H.; He, Y.; Zhou, W.; Bao, Y.; Chen, G.** (2018): Experimental and numerical investigations of the dynamic responses of an asymmetrical arch railway bridge. *Proceedings of the Institution of Mechanical Engineers, Part F: Journal of Rail and Rapid Transit*, vol. 232, no. 9, pp. 2309-2323.
- Gou, H.; Long, H.; Bao, Y.; Chen, G.; Pu, Q. et al.** (2018): Stress distributions in girder-arch-pier connections of long-span continuous rigid frame arch railway bridges. *Journal of Bridge Engineering*, vol. 23, no. 7, 04018039.
- Gou, H.; Shi, X.; Zhou, W.; Cui, K.; Pu, Q.** (2018): Dynamic performance of continuous railway bridges: Numerical analyses and field tests. *Proceedings of the Institution of Mechanical Engineers, Part F: Journal of Rail and Rapid Transit*, vol. 232, no. 3, pp. 936-955.
- Gou, H.; Yang, B.; Guo, W.; Biao, Y.** (2019): Static and dynamic responses of a tied-arch railway bridge under train load. *Structural Engineering and Mechanics*, vol. 71, no. 1, pp. 13-22.
- Gou, H.; Yang, L.; Mo, Z.; Guo, W.** (2019): Effect of long-term bridge deformations on safe operation of high-speed railway and vibration of vehicle-bridge coupled system. *International Journal of Structural Stability and Dynamics*.
- Gou, H.; Zhou, W.; Chen, G.; Bao, Y.; Pu, Q.** (2018): In-situ test and dynamic response of a double-deck tied-arch bridge. *Steel and Composite Structures*, vol. 27, no. 2, pp. 161-175.
- Grigorian, C. E.; Yang, T. S.; Popov, E. P.** (1993): Slotted bolted connection energy dissipators. *Earthquake Spectra*, vol. 9, no. 3, pp. 491-504.
- Gu, Q.; Liu, Y.; Guo, W.; Li, W.; Yu, Z. et al.** (2019): A practical wheel-rail interaction element for modeling vehicle-track-bridge systems. *International Journal of Structural Stability and Dynamics*, vol. 19, no. 2, 1950011.
- Guo, W.; Hu, Y.; Liu, H.; Bu, D.** (2019): Seismic performance evaluation of typical piers of China's high-speed railway bridge line using pushover analysis. *Mathematical Problems in Engineering*, pp. 1-17.
- Guo, W.; Wu, J.; Hu, Y.; Li, Y.; Yang, T. Y.** (2019): Seismic performance evaluation of typical dampers designed by Chinese building code. *Earthquake Engineering and Engineering Vibration*, vol. 18, no. 2, pp. 433-446.
- Guo, W.; Zhai, Z.; Cui, Y.; Yu, Z.; Wu, X.** (2019): Seismic performance assessment of low-rise precast wall panel structure with bolt connections. *Engineering Structures*, vol. 181, pp. 562-578.

Guo, W.; Zhai, Z.; Wang, H.; Liu, Q.; Xu, K. et al. (2019): Shaking table test and numerical analysis of an asymmetrical twin-tower super high-rise building connected with long-span steel truss. *Structural Design of Tall and Special Buildings*, e1630.

Guo, W.; Zhai, Z.; Yu, Z.; Chen, F.; Gong, Y. et al. (2019): Experimental and numerical analysis of the bolt connections in a low-rise precast wall panel structure system. *Advances in Civil Engineering*, vol. 2019, pp. 1-23.

Guo, W.; Zhai, Z.; Yu, Z.; Long, Y. (2019): Facility performance indexes and rapid test feasibility evaluation method of shaking tables. *KSCCE Journal of Civil Engineering*, vol. 23, no. 7, pp. 3097-3112.

Guo, Z.; Jeng, D. S.; Zhao, H.; Guo, W.; Wang, L. (2019): Effect of seepage flow on sediment incipient motion around a free spanning pipeline. *Coastal Engineering*, vol. 143, pp. 50-62.

Hou, W.; Li, Y.; Guo, W.; Li, J.; Chen, Y. et al. (2018): Railway vehicle induced vibration energy harvesting and saving of rail transit segmental prefabricated and assembling bridges. *Journal of Cleaner Production*, vol. 182, pp. 946-959.

Jiang, L.; Shao, G.; Jiang, J.; Wang, H. (2013): Experimental study on seismic performance of solid piers with round ended cross-section in high-speed railway. *China Civil Engineering Journal*, vol. 46, no. 3, pp. 86-95.

Kang, X.; Jiang, L.; Bai, Y.; Caprani, C. C. (2017): Seismic damage evaluation of high-speed railway bridge components under different intensities of earthquake excitations. *Engineering Structures*, vol. 152, pp. 116-128.

Kim, J.; Shin, H. (2017): Seismic loss assessment of a structure retrofitted with slit-friction hybrid dampers. *Engineering Structures*, vol. 130, pp. 336-350.

Kim, S. H.; Mha, H. S.; Lee, S. W. (2006): Effects of bearing damage upon seismic behaviors of a multi-span girder bridge. *Engineering structures*, vol. 28, no. 7, pp. 1071-1080.

Li, K.; Guo, Z.; Wang, L.; Jiang, H. (2019): Effect of seepage flow on shields number around a fixed and sagging pipeline. *Ocean Engineering*, vol. 172, pp. 487-500.

Liu, H.; Yu, Z.; Guo, W. (2019): A fast modeling technique for the vertical train-track-bridge interactions. *Shock and Vibration*, pp. 1-14.

Martínez-Rodrigo, M. D.; Filiatrault, A. (2015): A case study on the application of passive control and seismic isolation techniques to cable-stayed bridges: a comparative investigation through non-linear dynamic analyses. *Engineering Structures*, vol. 99, pp. 232-252.

Metin, M.; Ulu, A.; Paksoy, M.; Yücel, M. E. (2017): Vibration mitigation of railway bridge using magnetorheological damper. *Modern Railway Engineering*, pp.17-29.

Ministry of Construction (2006): GB50111-2006, Code for Seismic Design of Railway Engineering.

Ministry of Railways (2004): Pot Bearings for Railway Bridge TB/T 2331-2004.

Mirzabagheri, S.; Sanati, M.; Aghakouchak, A. A.; Khadem, S. E. (2015): Experimental and numerical investigation of rotational friction dampers with multi units in

steel frames subjected to lateral excitation. *Archives of Civil and Mechanical Engineering*, vol. 15, no. 2, pp. 479-491.

Monir, H. S.; Zeynali, K. (2013): A modified friction damper for diagonal bracing of structures. *Journal of Constructional Steel Research*, vol. 87, pp. 17-30.

Mualla, I. H.; Belev, B. (2002): Performance of steel frames with a new friction damper device under earthquake excitation. *Engineering Structures*, vol. 24, no. 3, pp. 365-371.

Mualla, I.; Belev, B. (2015): Analysis, design and applications of rotational friction dampers for seismic protection. *Czasopismo Inżynierii Lądowej, Środowiska i Architektury*, vol. 62, no. 4, pp. 335-346.

Pall, A. S.; Marsh, C. (1982): Response of friction damped braced frames. *Journal of Structural Engineering*, vol. 108, no. 9, pp. 1313-1323.

Rådeström, S.; Ülker-Kaustell, M.; Andersson, A.; Tell, V.; Karoumi, R. (2017): Application of fluid viscous dampers to mitigate vibrations of high-speed railway bridges. *International Journal of Rail Transportation*, vol. 5, no. 1, pp. 47-62.

Ren, J.; Li, X.; Yang, R.; Wang, P.; Xie, P. (2016): Criteria for repairing damages of CA mortar for prefabricated framework-type slab track. *Construction and Building Materials*, vol. 110, pp. 300-311.

Ruan, B. (1985): The torque coefficient of bolt. *Engineering Mechanics*, vol. 2, no. 2, pp. 132-137.

Shrestha, B.; Hao, H.; Bi, K. (2017): Devices for protecting bridge superstructure from pounding and unseating damages: an overview. *Structure and Infrastructure Engineering*, vol. 13, no. 3, pp. 313-330.

Shrestha, B.; Hao, H.; Ibrahim, N. H.; Bi, K. (2016): On the effectiveness of rotational friction hinge damper to control responses of multi-span simply supported bridge to non-uniform ground motions. *Advances in Structural Engineering*, vol. 19, no. 10, pp. 1575-1591.

Yan, B.; Huang, J.; Liu, S.; Lou, P. (2018): Seismic responses of CRTS-II track system on bridge under complex geography conditions. *Journal of Traffic & Transportation Engineering*, vol. 18, no. 1, pp. 42-50.

Yan, B.; Dai, G. L.; Hu, N. (2015): Recent development of design and construction of short span high-speed railway bridges in China. *Engineering Structures*, vol. 100, pp. 707-717.

Yan, B.; Liu, S.; Dai, G.; Pu, H.; Tang, J. (2016): Nonlinear interaction between CRTS-II ballastless track and bridges due to multi-dimensional earthquake. *Journal of the China Railway Society*, vol. 38, no. 5, pp. 74-80.

Yan, B.; Liu, S.; Pu, H.; Dai, G.; Cai, X. (2017): Elastic-plastic seismic response of CRTS II slab ballastless track system on high-speed railway bridges. *Science China Technological Sciences*, vol. 60, no. 6, pp. 865-871.

Yu, Z.; Liu, H.; Guo, W.; Liu, Q. (2017): A general spectral difference method for calculating the minimum safety distance to avoid the pounding of adjacent structures during earthquakes. *Engineering Structures*, vol. 150, pp. 646-655.

Zeng, Z. P.; He, X. F.; Zhao, Y. G.; Yu, Z. W.; Chen, L. K. et al. (2015): Random vibration analysis of train-slab track-bridge coupling system under earthquakes. *Structural Engineering and Mechanics*, vol. 54, no. 5, pp. 1017-1044.

Zhu, Q.; Dai, G.; Yan, B. (2014): Transfer law of breaking force between simply-supported bridges and CRTS II slab ballastless track. *Journal of Railway Science and Engineering*, vol. 11, pp. 13-19.

Zhu, S.; Yang, J.; Yan, H.; Zhang, L.; Cai, C. (2015): Low-frequency vibration control of floating slab tracks using dynamic vibration absorbers. *Vehicle System Dynamics*, vol. 53, no. 9, pp. 1296-1314.

Zhu, Z.; Gong, W.; Wang, L.; Bai, Y.; Yu, Z. et al. (2019): Efficient assessment of 3D train-track-bridge interaction combining multi-time-step method and moving track technique. *Engineering Structures*, vol. 183, pp. 290-302.

Zhu, Z.; Gong, W.; Wang, L.; Li, Q.; Bai, Y. et al. (2018): An efficient multi-time-step method for train-track-bridge interaction. *Computers & Structures*, vol. 196, pp. 36-48.